PIER C

(Received 20 April 2025, Accepted 3 June 2025, Scheduled 9 June 2025)

Quasi-Z-Source Inverter Model Predictive Control Strategy with Improved Switching Sequence

Yang Zhang[1], Yuwei Meng[1], Xiuhai Yang[1], Dingai Zhong[1], and Zhun Cheng[2,*]

[1]*Hunan University of Technology, Zhuzhou 412007, China*
[2]*Hunan Railway Professional Technology College, Zhuzhou 412001, China*

ABSTRACT: To address the issue of large inductor current ripple in the existing finite switching sequence model predictive control (FSS-MPC) strategy for quasi-Z-source inverters (qZSI), an improved switching sequence model predictive control strategy is proposed. First, the switching sequences and inductor current ripple characteristics of the existing strategy are analyzed. Then, the voltage vectors are rearranged, and eight switching sequences with shoot-through vectors are designed within one sector. Next, the duty cycles of the voltage vectors are calculated based on the inverse relationship between the duty cycle and cost function value. Additionally, a weighting coefficient for switching times is introduced into the cost function. Finally, simulations and experiments are conducted to compare the proposed method with the conventional FSS-MPC strategy. The results verify the feasibility and effectiveness of the proposed control strategy.

1. INTRODUCTION

As the core interface device in renewable energy grid-connected systems, inverters perform the critical task of power conversion. The current mainstream technologies primarily include voltage source inverters (VSIs) and current source inverters (CSIs). However, their output voltage is typically equal to or lower than the input voltage, lacking the capability to achieve both boosting and bucking operations simultaneously.

In response to the technical limitations of conventional inverters, Z-Source Inverter (ZSI) realizes voltage amplitude boosting and bucking regulation by introducing LC impedance units. ZSI topology offers advantages including simple structure, low cost, and high energy conversion efficiency [1–3]. Its unique shoot-through operation mode also eliminates the need for dead-time setting in traditional inverters. However, practical applications of ZSI face challenges such as discontinuous input current and high voltage stress on power devices. To overcome these limitations, quasi-Z-source inverter (qZSI) was developed by reconstructing an impedance network. qZSI achieves continuous input current and reduced voltage stress on power devices. Moreover, qZSI demonstrates significant advantages in power quality improvement and exhibits wide boosting/bucking capability in modern power systems [4, 5].

With the continuous advancement of power electronics technology, conventional control methods can no longer meet modern power systems' requirements for dynamic performance, precise regulation, and multi-objective optimization. Model predictive control (MPC), as an advanced nonlinear control strategy with excellent dynamic optimization capabilities, has gradually become a mainstream method for renewable energy grid-connected inverter control [6, 7]. MPC employs real-time system data and predictive models to perform rolling optimization, enabling the system to make predictive control decisions over future time steps. Compared with traditional control methods, MPC achieves precise regulation of multiple variables including voltage, frequency, and power while handling complex system constraints and nonlinearities. Consequently, MPC enhances system stability while reducing energy consumption and control complexity [8, 9].

In [10, 11], a two-vector MPC strategy is employed for voltage source inverters, where two voltage vectors are utilized in each sampling period to optimize current control. In [12], a three-vector model predictive current control strategy is proposed. This strategy generates six desired voltage vectors with adjustable directions and magnitudes, covering arbitrary directions and amplitudes, which significantly reduces current harmonics. Although these multi-vector MPC methods contribute to improved dynamic and steady-state control performance, they are accompanied by issues such as heavy computational burden. To optimize these multi-vector MPC approaches, a novel modulated model predictive control (M^2PC) method is presented in [13, 14]. This strategy maintains control performance while reducing computational load. The method proposed in [13, 14] determines the duty cycle of each voltage vector based on its cost function value, where an inverse relationship between the duty cycle and cost function value is established. This calculation method is characterized by easy implementation, low computational complexity, and effective avoidance of over-modulation. In addition, a two-step MPC strategy [15] provides a balanced optimization approach for dynamic systems by limiting adjacent switching vectors to reduce switching frequency while maintaining control performance.

* Corresponding author: Zhun Cheng (120277982@qq.com).

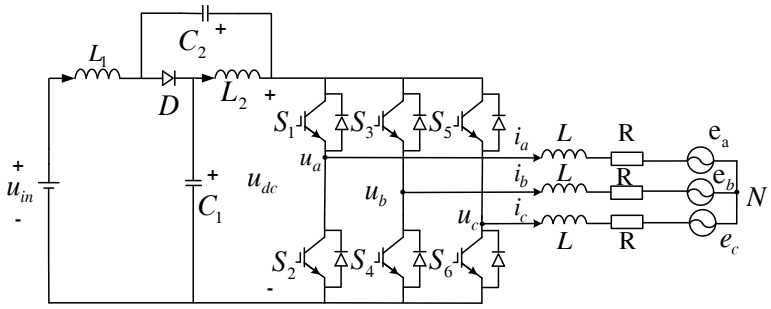

FIGURE 1. qZSI main circuit.

The conventional finite control set model predictive control (FCS-MPC) strategy is characterized by variable switching frequency and high sampling frequency requirements. To address these issues, the finite switching sequence model predictive control (FSS-MPC) strategy is proposed by researchers. In [16], a grid-connected inverter FSS-MPC strategy is presented, where optimized switching sequences are designed through rearrangement of space voltage vector combinations, resulting in reduced switching transitions and improved spectral distribution. In [17], an FSS-MPC strategy for permanent magnet synchronous motors is proposed. The torque control without weight adjustment is achieved through optimized design of the control objective function. In [18], a model predictive direct power control method is proposed for single-phase three-level pulse rectifiers. The control strategy is implemented by incorporating MPC principles into direct power control, with simplified switching sequence selection employed to reduce algorithm complexity. In [19], an FSS-MPC strategy for pulse width modulation (PWM) rectifiers is proposed. Fixed switching frequency is obtained through finite control set optimization and multi-vector synthesis. Recent MPC research has focused on finding a balance among switching losses, computational complexity, and control performance. Ref. [20] reviews strategies such as modulation-based MPC and switching sequence-optimized MPC for permanent magnet synchronous motor drive systems and summarizes strategies regarding computational complexity and switching frequency aspects, among others. The above literature mainly focuses on two-level inverters or PMSMs but does not address the optimization of the shoot-through state of qZSI, whose control strategy cannot be directly migrated to the qZSI containing the shoot-through state. Furthermore, qZSI needs to balance the switching continuity between the shoot-through vector and non-shoot-through vector. In [21], a quasi-Z-source based FSS-MPC direct power control strategy is proposed. Although output current harmonic distortion is reduced by this method, excessive inductor current ripple amplitude is observed. More importantly, the inductor in quasi-Z-source inverter occupies a significant portion of the total volume. To maintain identical inductor current ripple and output voltage, the inductor size in quasi-Z-source inverters is approximately 1.27 times larger than that in conventional inverters [22]. Therefore, the reduction of inductor current ripple is essential.

To improve the issue of large inductor current ripple in existing finite switching sequence model predictive control, this paper proposes an improved FSS-MPC strategy for quasi-Z-source inverter. The proposed strategy effectively suppresses inductor current ripple in qZSI while simultaneously improving output current harmonic characteristics through optimized switching sequence design. The main contributions of this study include:

1) First, the shoot-through vector is divided into four segments. By rationally distributing shoot-through vectors within the switching sequences, the problem of large inductor current ripple is resolved.

2) Second, the vector arrangement is reconstructed. Eight optimized switching sequences containing shoot-through vectors are designed within each sector. To balance switching losses, a switching frequency weighting coefficient is introduced into the cost function, achieving optimal trade-off between control performance and switching losses.

3) Finally, the modulated model predictive control method is adopted to simplify calculations. Each designed switching sequence consists of three active voltage vectors and corresponding shoot-through vectors. The computational complexity is reduced through optimized duty cycle calculation.

2. WORKING PRINCIPLE

The quasi-Z-source inverter is a quasi-Z-source network added between the DC input voltage (u_{in}) of the conventional inverter and the inverter bridge arm. The main circuit of the quasi-Z-source inverter is shown in Figure 1, which mainly consists of a DC power supply, a quasi-Z-source network, an inverter bridge, an equivalent filtering inductor (L), and an equivalent resistor (R). The quasi-Z-source network consists of two capacitors ($C_1 = C_2$) and two inductors, ($L_1 = L_2$). Since the DC power supply u_{in} is connected in series with the inductor L_1, the quasi-Z-source inverter can be made to maintain the continuity of the input current during operation.

The predicted value of the output current is obtained from Figure 1:

$$i_{(\alpha,\beta)}(k+1)=\left(1-\frac{RT_s}{L}\right)i_{(\alpha,\beta)}(k)+\frac{T_s}{L}(u_{(\alpha,\beta)}(k)-e_{(\alpha,\beta)}(k)) \quad (1)$$

where $i_{(\alpha,\beta)}(k)$, $u_{(\alpha,\beta)}(k)$, and $e_{(\alpha,\beta)}(k)$ are the output current, output voltage, and grid voltage components of the kth

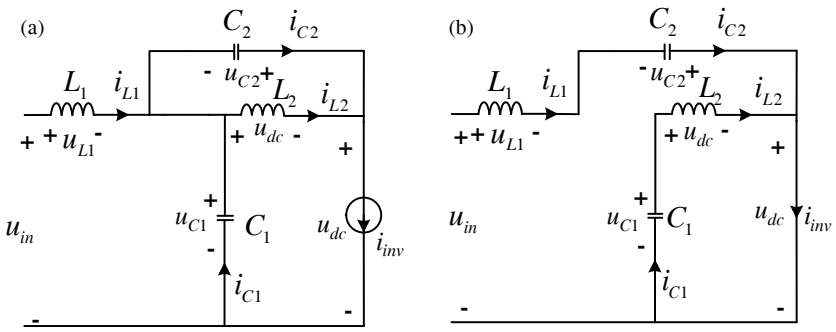

FIGURE 2. Two operating states of quasi-Z-source inverter. (a) Non-shoot-through state. (b) Shot-through state.

sampling period on the $\alpha\beta$ coordinate system; $i_{(\alpha,\beta)}(k+1)$ is the predicted output current component of the $k+1$th sampling period on the $\alpha\beta$ coordinate system; and T_s is the sampling period.

The space vectors of the output voltages of the quasi-Z-source inverter for different switching combinations are given in Table 1. Combined with Table 1, the output voltage vector of the quasi-Z source inverter is:

$$u_x = \frac{2u_{\mathrm{dc}}}{3}\left(S_{\mathrm{a}} + aS_{\mathrm{b}} + a^2 S_{\mathrm{c}}\right) \tag{2}$$

where u_{dc} is the DC chain voltage $a = \mathrm{e}^{\mathrm{j}2\pi/3}$, and $x = [0,1,2,3,4,5,6,7]$, S_A, S_B, S_C are the switching states of phases A, B, and C, respectively.

TABLE 1. Different switching states of quasi-Z-source inverter.

vector	S_1	S_2	S_3	S_4	S_5	S_6
U_0	0	0	0	1	1	1
U_1	1	0	0	0	1	1
U_2	1	1	0	0	0	1
U_3	0	1	0	1	0	1
U_4	0	1	1	1	0	0
U_5	0	0	1	1	1	0
U_6	1	0	1	0	1	0
U_7	1	1	1	0	0	0
Shoot-through vector	1	1	1	1	1	1
Shoot-through vector	1	1	X	$\bar{X}$	X	$\bar{X}$
Shoot-through vector	X	$\bar{X}$	1	1	X	$\bar{X}$
Shoot-through vector	X	$\bar{X}$	X	$\bar{X}$	1	1

The quasi-Z-source inverter incorporates a quasi-Z-source network with inductors and capacitors, which enables active triggering of bridge shoot-through states during specific periods. This shoot-through capability provides functions unattainable by conventional inverters. By switching between shoot-through and non-shoot-through states in the three-phase bridge, the qZSI controls energy storage and release in the inductors and capacitors. This operation boosts the DC-link voltage during non-shoot-through state, achieving voltage step-up functionality. The equivalent circuits of the qZSI in non-shoot-through and shoot-through states are shown in Figure 2(a) and Figure 2(b), respectively.

3. EXISTING FSS-MPC STRATEGY

FCS-MPC evaluates all possible switching state combinations of the inverter in each control cycle. It predicts the system's dynamic response and selects the optimal switching state based on cost function evaluation, which is directly applied to the power switches. However, the computational burden increases significantly with the number of switching states. In contrast, FSS-MPC outputs a predefined switching sequence in each sampling cycle. This sequence consists of voltage vectors switched in a specific order. By optimizing the arrangement of switching sequences, FSS-MPC maintains control performance while improving key indicators like switching frequency and current ripple.

3.1. Voltage Vector Sequence

The voltage vectors applied in qZSI must include both active vectors and shoot-through vectors. In conventional FSS-MPC, each switching sequence contains three basic voltage vectors and one shoot-through vector $U_{sh0}(111111)$. Additionally, a shoot-through vector is inserted between every active vector and zero vector within each control cycle.

The existing FSS-MPC employs six switching sequences (I to VI) as follows:

Switching sequence I: $U_1 \to U_2 \to U_{sh0} \to U_7 \to U_{sh0} \to U_2 \to U_1$; Switching sequence II: $U_3 \to U_2 \to U_{sh0} \to U_7 \to U_{sh0} \to U_2 \to U_3$; Switching sequence III: $U_3 \to U_4 \to U_{sh0} \to U_7 \to U_{sh0} \to U_4 \to U_3$; Switching sequence IV: $U_5 \to U_4 \to U_{sh0} \to U_7 \to U_{sh0} \to U_4 \to U_5$; Switching sequence V: $U_5 \to U_6 \to U_{sh0} \to U_7 \to U_{sh0} \to U_6 \to U_5$; switching sequence VI: $U_1 \to U_6 \to U_{sh0} \to U_7 \to U_{sh0} \to U_6 \to U_1$. Taking switching sequence I as an example, the synthesized voltage vector V_{ref} is:

$$V_{\mathrm{ref}} = U_1T_1/T_s + U_2T_2/T_s + U_7T_0/T_s + U_{\mathrm{sh0}}T_{\mathrm{sh}}/T_s \tag{3}$$

where T_{sh} and T_0 are the durations of the shoot-through vector and zero vector, respectively, and have $T_{sh} = d_{sh} \times T_s$, and d_{sh} is the shoot-through duty cycle. The existing FSS-MPC voltage vector action time is calculated using the differential beat free control.

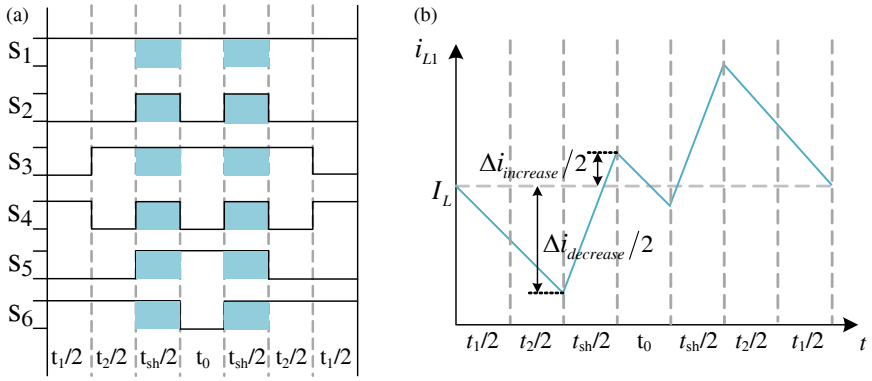

FIGURE 3. Switching sequence I waveform. (a) Switching state. (b) Inductive current waveform.

The switching action of the existing FSS-MPC's switching sequence I in one sampling cycle is shown in Figure 3(a), and its inductor current ripple characteristics are shown in Figure 3(b). The analysis shows that a total of 16 on-state changes of all switching elements occur in each sampling cycle, resulting in frequent switching. The number of times that the inductor current rises and falls in a sampling cycle is 5 in total.

3.2. Inductor Current Ripple Calculation

In quasi-Z-source inverter, the inductor current energy release duration equals the shoot-through time when i_{L1} decreases, while the energy storage duration equals the non-shoot-through time when i_{L1} increases.

The inductor current ripple at energy release is:

$$\Delta i_{\text{decrease}} = \frac{d_{sh} u_{\text{dc}}}{L_1} T_1 + T_2 \tag{4}$$

The inductor current ripple during energy storage is:

$$\Delta i_{\text{increase}} = \frac{d_{sh} u_{dc}}{L_1} T_0 \tag{5}$$

From the variation rule of each vector in the general sector, the maximum inductor current ripple of the existing FSS-MPC strategy is:

$$\Delta I_{L\text{lmax}} = \max(\Delta i_{\text{decrease}}, \Delta i_{\text{increase}}) = \Delta i_{\text{decrease}} \tag{6}$$

4. IMPROVED FSS-MPC STRATEGY

4.1. Switching Sequence Optimization

The existing FSS-MPC strategy uses u_0 for all zero vector selections in each sector. In contrast, the improved FSS-MPC strategy expands the zero vector selections to both u_0 and u_7, while still maintaining three basic voltage vectors per control cycle. The alternating use of u_0 and u_7 balances device conduction time and prevents localized overheating caused by single zero vector application. For rapid voltage vector selection, the vector selection method is shown in Table 2, where reference voltage vectors in sector I utilize U_1 and U_2 as basic vectors combined with either U_0 or U_7 as zero vectors.

TABLE 2. Sector and voltage vector selection for reference voltage.

Sector	Effective vector	Zero vector
I	U_1, U_2	U_0 or U_7
II	U_2, U_3	U_0 or U_7
III	U_3, U_4	U_0 or U_7
IV	U_4, U_5	U_0 or U_7
V	U_5, U_6	U_0 or U_7
VI	U_6, U_1	U_0 or U_7

Based on the three-vector principle, eight distinct switching sequences can be designed per sector by selecting different vector combinations and arranging them in various orders. This diversity in switching sequences enhances control precision through increased selectivity.

For quasi-Z-source inverter, the load current remains continuous during both shoot-through vector and zero vector states. Therefore, replacing zero vectors with shoot-through vectors maintains AC-side output current stability while achieving effective voltage boosting. Shoot-through vectors are typically inserted between basic voltage vectors. Among various shoot-through implementation methods (including single or multiple bridge arm short-circuiting), single bridge arm short-circuiting is adopted to minimize unnecessary switching operations. The specific combinations of these sequences are shown in Figure 4.

Within a sampling period, different switching sequences make the number of device actions vary. This increase in the number of switching actions not only exacerbates the conduction loss and switching loss of the power semiconductor device, but also may increase the generation of high-frequency harmonics. Therefore, the switching sequence should be optimized to minimize the number of switching actions in each cycle, as well as to reduce the overall loss and optimize the power quality by reasonably selecting the switching sequences of adjacent cycles. Effective optimization ensures that the system improves efficiency while maintaining stability.

The new through vectors in switching sequence a to switching sequence h are U_{sh1}(110011), U_{sh2}(111001), U_{sh3}(110101), and U_{sh4}(100111). Table 3 shows the vector action sequence with the improved FSS-MPC using switching sequence I as an example.

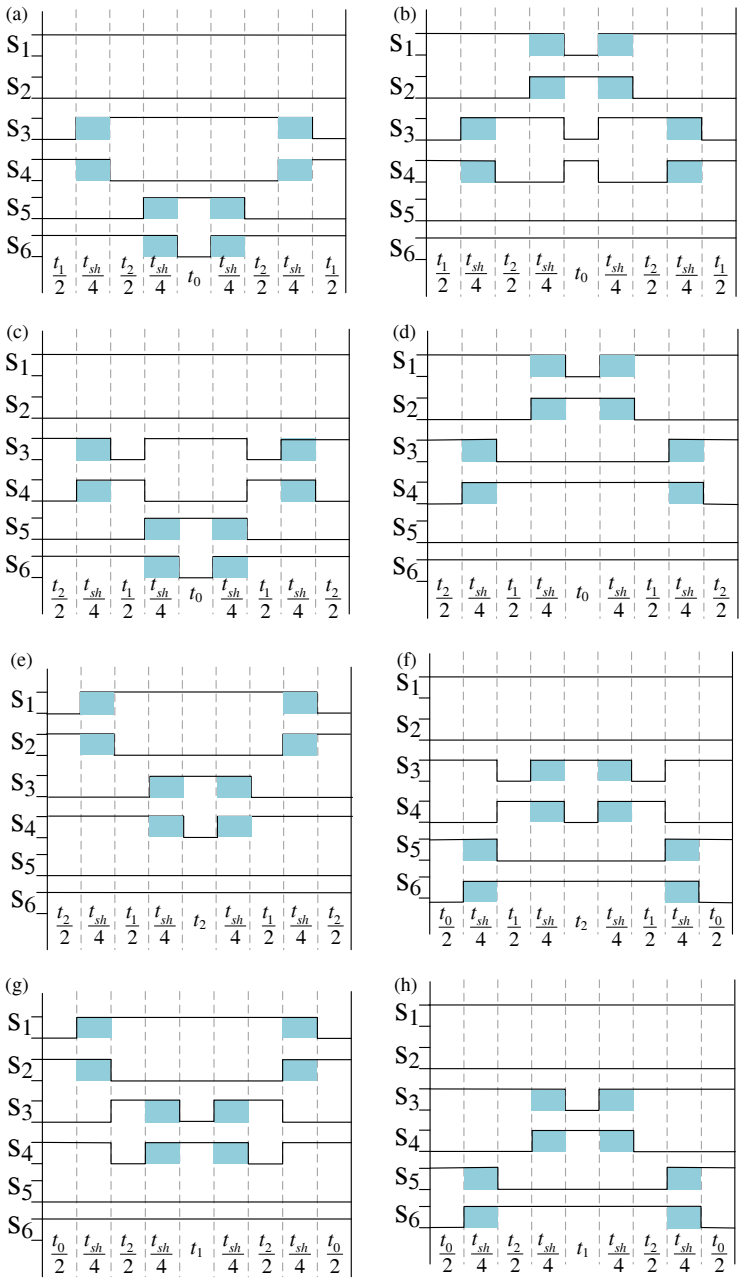

FIGURE 4. 8 switching sequences in sector I. (a) Switching sequence a. (b) Switching sequence b. (c) Switching sequence c. (d) Switching sequence d. (e) Switching sequence e. (f) Switching sequence f. (g) Switching sequence g. (h) Switching sequence h.

TABLE 3. Vector action sequence of switching sequence I.

Switching sequence	Vector action sequence
a	$U_1 \to U_{sh1} \to U_2 \to U_{sh2} \to U_7 \to U_{sh2} \to U_2 \to U_{sh1} \to U_1$
b	$U_1 \to U_{sh1} \to U_2 \to U_{sh3} \to U_0 \to U_{sh3} \to U_2 \to U_{sh1} \to U_1$
c	$U_2 \to U_{sh1} \to U_1 \to U_{sh2} \to U_7 \to U_{sh2} \to U_1 \to U_{sh1} \to U_2$
d	$U_2 \to U_{sh1} \to U_1 \to U_{sh4} \to U_0 \to U_{sh4} \to U_1 \to U_{sh1} \to U_2$
e	$U_0 \to U_{sh4} \to U_1 \to U_{sh1} \to U_2 \to U_{sh1} \to U_1 \to U_{sh4} \to U_0$
f	$U_7 \to U_{sh2} \to U_1 \to U_{sh1} \to U_2 \to U_{sh1} \to U_1 \to U_{sh2} \to U_7$
g	$U_0 \to U_{sh4} \to U_2 \to U_{sh1} \to U_1 \to U_{sh1} \to U_2 \to U_{sh4} \to U_0$
h	$U_7 \to U_{sh2} \to U_2 \to U_{sh1} \to U_1 \to U_{sh1} \to U_2 \to U_{sh2} \to U_7$

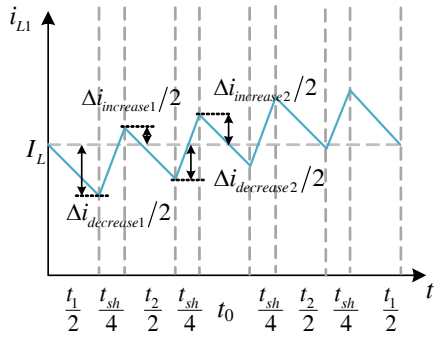

FIGURE 5. Sequence a inductor current waveform.

The inductor current waveform of the improved FSS-MPC switching sequence a is shown in Figure 5, where the number of times that the inductor current rises and falls in one sampling period is 9 in total.

Further analyzing the switching sequences b, c, f, and g in Figure 5, it can be seen that these sequences switch the on-state of all bridge arms a total of twelve times in one sampling cycle, which is four times more than the total switching times of switching sequences a, d, e, and h.

Model predictive control can identify the optimal switching sequence combination under multiple constraints, ensuring system control accuracy while maintaining efficient and stable operation. To solve the problem of high number of switches, the strategy proposed in this paper incorporates switching number constraint into the cost function. The introduction of this constraint can effectively limit the number of switching times, thus reducing the generation of unnecessary energy loss.

At the end of the k-*th* sampling period, the current switching state is analyzed. All possible switching sequences for the $(k+1)$-*th* moment are predicted, and the number of switching transitions N between adjacent cycles is calculated by counting state changes (e.g., a "1" to "0" transition counts as one switch). A corresponding cost function g_1 is constructed. During each sampling period, the algorithm evaluates all feasible switching sequence combinations, computes their g_1 values, and selects the optimal sequence with minimum g_1 as the execution scheme.

$$g_1 = [i_{\alpha\_ref} - i_\alpha\,(k+1)]^2 + [i_{\beta\_ref} - i_\beta\,(k+1)]^2 + \lambda_{\mathrm{N}} N_{\mathrm{switch}} \quad (7)$$

where λ_N is the weighting factor. If more attention is given to loss prioritization, the weighting factor needs to be increased to reduce the switching frequency. However, if the weighting factor is taken too large, the b, c, f, and g sequences will be excluded completely. If the output current performance and switching frequency need to be balanced, the weighting factor is not taken too large.

4.2. Calculation of Switching State Action Time

The proposed strategy utilizes three voltage vectors per sampling period. First, two adjacent active vectors (e.g., u_1, u_2) and a zero vector (u_0 or u_7) are selected according to the reference voltage vector's sector position. An optimization algorithm then calculates each vector's optimal duration. The switching state durations are determined by the inverse proportional relationship between duty ratios and cost function values, ensuring precise output current tracking of the reference value.

Its synthesized voltage vector can be expressed as the following mathematical expression:

$$u^* = d_i u_i + d_j u_j + d_k u_k + d_{sh} u_{sh} \quad (8)$$

where d_i, d_j, d_k are the two effective vector duty cycles and the zero vector duty cycle, respectively, where $d_i + d_j + d_k + d_{sh} = 1$. The duty cycle of each in the group of voltage vectors can be deduced from the method of calculating the duty cycle of M^{2}PC for each in the group of voltage vectors:

$$\begin{cases} d_i = \dfrac{(1-d_{sh})/g_{\mathrm{i}}}{1/g_{\mathrm{i}} + 1/g_{\mathrm{j}} + 1/g_{\mathrm{k}}} \\ d_{\mathrm{j}} = \dfrac{(1-d_{sh})/g_{\mathrm{j}}}{1/g_{\mathrm{i}} + 1/g_{\mathrm{j}} + 1/g_{\mathrm{k}}} \\ d_{\mathrm{k}} = \dfrac{(1-d_{sh})/g_{\mathrm{k}}}{1/g_{\mathrm{i}} + 1/g_{\mathrm{j}} + 1/g_{\mathrm{k}}} \end{cases} \quad (9)$$

where g_1, g_2, and g_3 are the cost functions obtained by substituting u_1, u_2, and u_3 into Equation (7), respectively. In order to realize the proposed strategy, first the vector duty cycle should be calculated and finally substituted into Equation (7), and the group with the smallest cost function value is selected to be applied to the inverter.

4.3. Inductor Current Ripple Calculation

The ripple of the inductor current in the energy release phase of the improved FSS-MPC strategy can be expressed as:

$$\begin{cases} \Delta i_{\mathrm{decrease1}} = \dfrac{d_{sh} u_{dc}}{L_1} T_1 \\ \Delta i_{\mathrm{decrease2}} = \left| \dfrac{d_{sh} u_{dc}}{L_1}(T_1 + T_2) - \dfrac{(1-d_{sh}) u_{dc}}{2L_1} T_{\mathrm{sh}} \right| \end{cases} \quad (10)$$

The ripple of the inductor current during the energy storage phase can be expressed as:

$$\begin{cases} \Delta i_{\mathrm{increase1}} = \left| \dfrac{d_{sh} u_{\mathrm{dc}}}{L_1} T_1 - \dfrac{(1-d_{sh}) u_{\mathrm{dc}}}{2L_1} T_{\mathrm{sh}} \right| \\ \Delta i_{\mathrm{increase2}} = \left| \dfrac{d_{sh} u_{\mathrm{dc}}}{L_1}(T_1 + T_2) - \dfrac{(1-d_{sh}) u_{\mathrm{dc}}}{L_1} T_{\mathrm{sh}} \right| \end{cases} \quad (11)$$

Therefore the proposed finite switching sequence model predicts the peak current ripple amplitude that can be achieved by the control strategy:

$$\begin{aligned} \Delta i_{L\mathrm{lmax}} &= \max(\Delta i_{\mathrm{decrease1}}, \Delta i_{\mathrm{decrease2}}, \Delta i_{\mathrm{increase1}}, \Delta i_{\mathrm{increase2}}) \\ &= \max(\Delta i_{\mathrm{decrease1}}, \Delta i_{\mathrm{decrease2}}) \end{aligned} \quad (12)$$

According to the formula analysis, under the same system parameters, the proposed improved FSS-MPC strategy can effectively reduce the ripple of the inductor current compared to the existing method. In summary, the algorithmic control flowchart of the improved FSS-MPC strategy is shown in Figure 6.

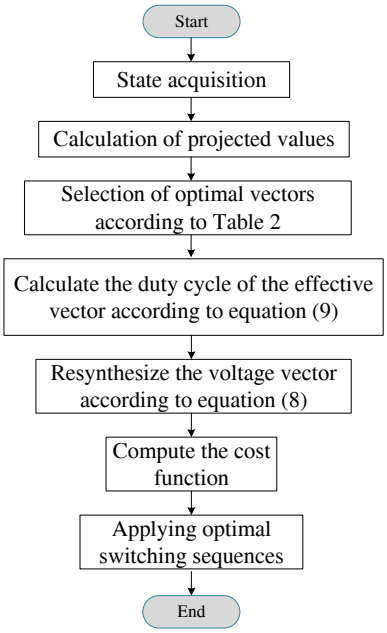

FIGURE 6. Control flowchart of the proposed FSS-MPC strategy algorithm.

5. SIMULATION AND EXPERIMENTAL VERIFICATION

The complete quasi-Z-source inverter system model was first developed in Matlab/Simulink simulation environment. Subsequently, its hardware implementation was built on an RT-LAB (OP5600) platform, as shown in Figure 7. Comparative verification was conducted between the conventional FSS-MPC strategy and the improved FSS-MPC strategy for steady-state performance evaluation. All simulations and experimental validations were performed at $f = 50$ Hz, with detailed data presented in Table 4.

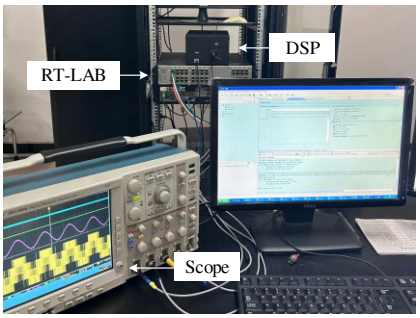

FIGURE 7. RT-LAB experiment platform.

TABLE 4. Experimental parameters.

Parameters	Values
Grid line voltage (e)	380 V
qZSI inductance (L_1, L_2)	3 mH
qZSI capacitance (C_1, C_2)	3000 μF
Filter inductors (L)	3 mH
Filter capacitor (C)	100 μF

With the DC-link voltage reference set to 300 V, Figure 8 presents the experimental waveforms of DC-link voltage (u_{dc}) and inductor current (i_{L1}) obtained using both finite switching sequence model predictive control strategy at 10 kHz sampling frequency. Experimental results demonstrate stable regulation of u_{dc} at 300 V with an average inductor current (i_{L1ref}) of 5 A. Comparative analysis reveals that while both control methods achieve effective reference tracking, the proposed improved FSS-MPC strategy shows superior performance in inductor current ripple suppression, exhibiting smaller peak-to-peak ripple than the conventional approach.

As shown in Figure 9, the inverter DC chain voltage u_{dc} and inductor current i_{L1} are shown in four sampling periods, and it can be seen that the inductor undergoes four complete charging and discharging processes in each sampling period. The inductor is also in the energy storage stage in the shoot-through state, and its current grows linearly, at which time the DC chain voltage drops to zero potential, while in the non-shoot-through state, the inductor releases energy; the current shows a decreasing trend; the DC chain voltage is restored to the rated value of 300 V; and the system enters the normal conduction state. The peak inductor current ripple of the existing FSS-MPC strategy is 0.55 A, and the peak inductor current ripple of the improved FSS-MPC strategy is 0.31 A. Under the same operating conditions, the peak inductor current ripple is reduced by about 44% with the proposed optimized control scheme. The effectiveness of the proposed improved FSS-MPC strategy in reducing the inductor current ripple is verified.

From the experimental results shown in Figure 10, it can be concluded that the peak amplitude of the three-phase output current is maintained at about 5 A, while the peak value of the grid voltage waveform reaches 311 V. The grid voltage e_a is in phase with the output current i_a.

Figure 11 shows the harmonic spectrum comparison of the two control strategies. The THD of the existing FSS-MPC strategy is 2.62%, and the THD of the improved FSS-MPC strategy is reduced to 2.02%. The amplitude of low harmonics is reduced; the distribution of high harmonics is more dispersed; and their amplitudes are further reduced. The reduction in THD confirms that the improved strategy can effectively suppress harmonic pollution, enhance output current waveform quality, and comply with grid harmonic standards.

The THD reduction of the improved strategy can reduce the additional loss caused by current harmonics, improve the system efficiency, reduce the temperature rise of the inductor and core loss, and prolong the life of the device. The decentralization of high-frequency harmonic amplitude reduces the switching stress of power devices and lowers the risk of device failure. The improved strategy expands the search space of the controller by rolling optimization with multiple switching sequences, and at the same time improves the system control accuracy. The strategy still maintains the high accuracy control performance after the introduction of the switching times weighting coefficients.

The simulated waveforms of switching tube conduction of the proposed control strategy for one sampling period from sequence a to sequence h in sector I are shown in Figure 12, where

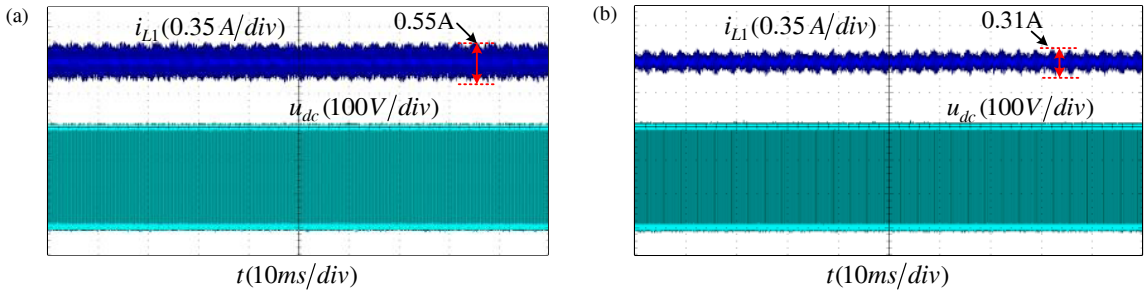

FIGURE 8. Inverter DC chain voltage u_{dc} and inductor current i_{L1} waveforms. (a) Existing FSS-MPC strategy. (b) Improved the FSS-MPC strategy.

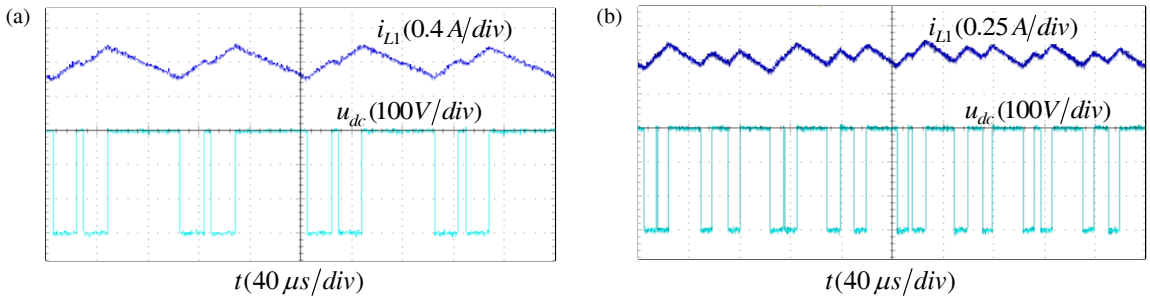

FIGURE 9. DC chain voltage u_{dc} and inductor current i_{L1} waveforms for four control cycles. (a) Existing FSS-MPC strategy. (b) Improved the FSS-MPC strategy.

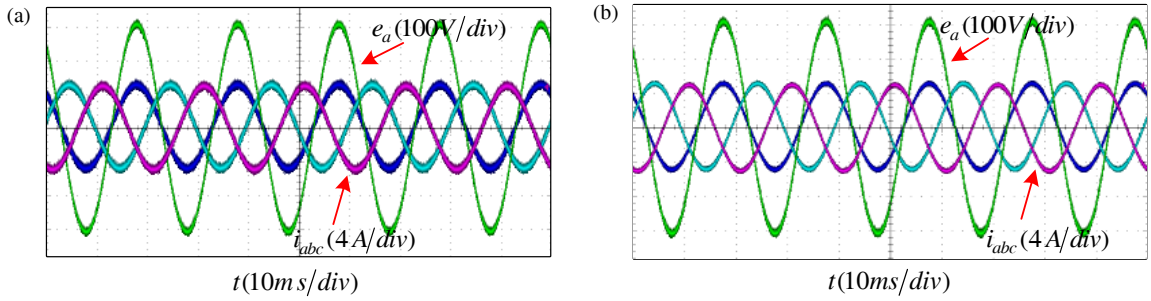

FIGURE 10. Grid voltage e_a and three-phase grid-connected current i_{abc}. (a) Existing FSS-MPC strategy. (b) Improved the FSS-MPC strategy.

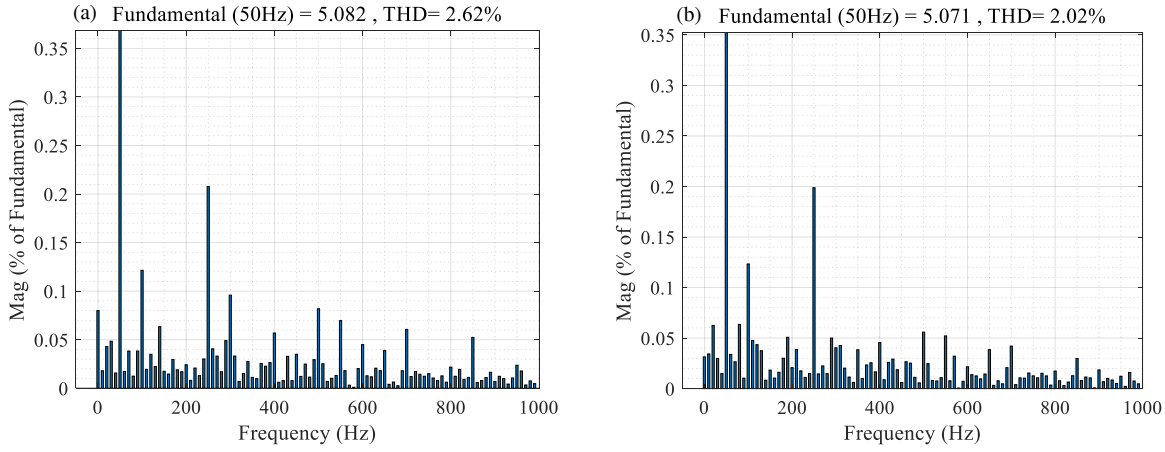

FIGURE 11. Harmonic waveforms for both strategies. (a) Existing FSS-MPC strategy. (b) Improved the FSS-MPC strategy.

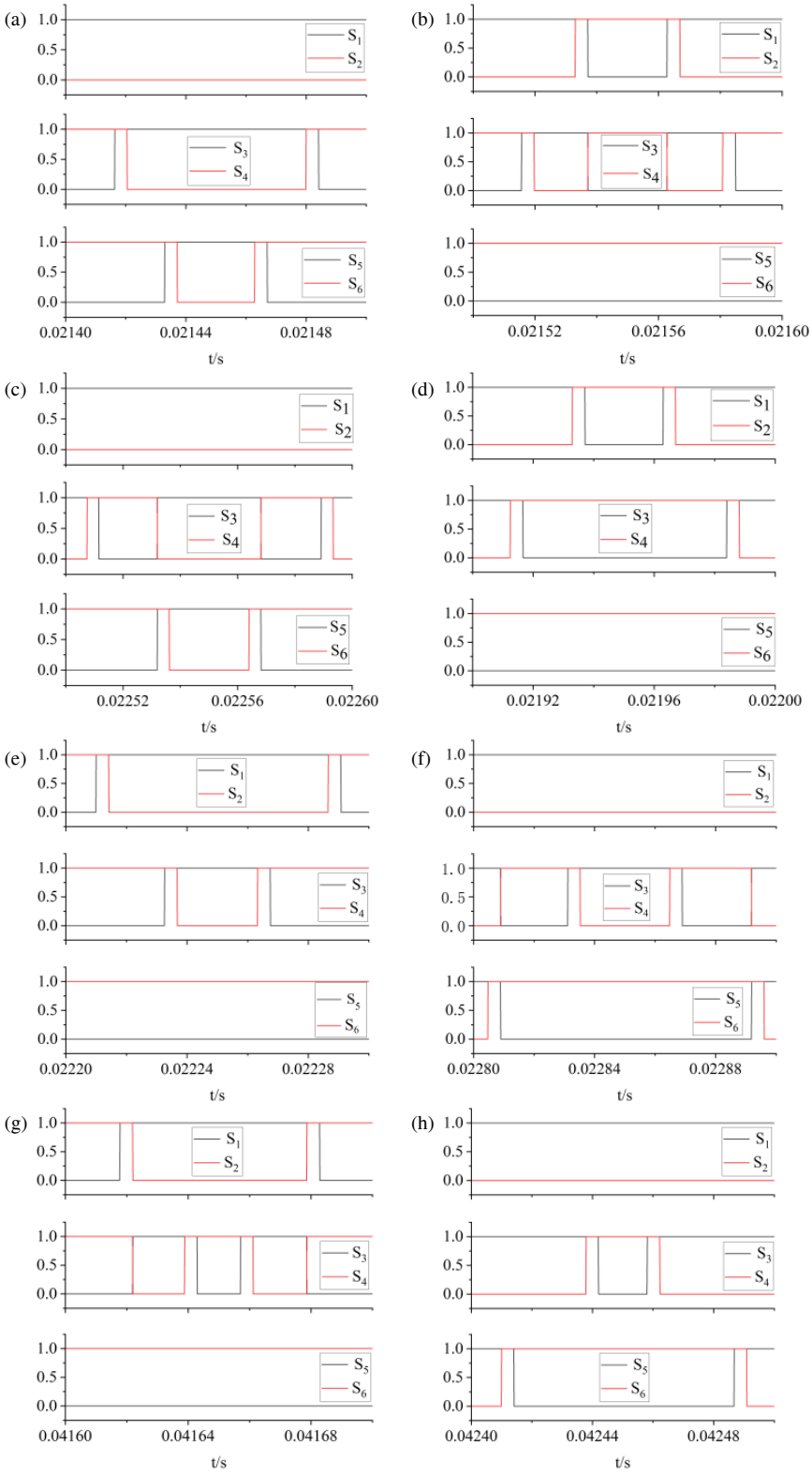

FIGURE 12. Simulated waveforms of switching tube conduction states for eight switching sequences in sector I. (a) Switching sequence a. (b) Switching sequence b. (c) Switching sequence c. (d) Switching sequence d. (e) Switching sequence e. (f) Switching sequence f. (g) Switching sequence g. (h) Switching sequence h.

the vertical coordinate is the switching state (1 = conducting, 0 = off).

The simulation waveforms of the switching devices show that, from top to bottom, are the conduction states of switching tubes S_1 to S_6, respectively. When both the upper and lower switching tubes conduct simultaneously, the system enters the shoot-through state. The simulation results demonstrate that

TABLE 5. Performance comparison of control strategies.

Metric	Existing FSS-MPC strategy	Improved FSS-MPC	Improvement
Output current THD	2.62%	2.02%	23% Reduction
Inductive current ripple (Peak-to-peak)	0.55 A	0.31 A	44% Reduction
Average switching frequency	15 kHZ	9.3 kHZ	38% Reduction

the improved FSS-MPC strategy achieves four shoot-through states in each sampling period.

Table 5 shows a comparison table of the experimental results of the two strategies. The experimental results show that compared with the existing FSS-MPC strategy, the average switching frequency of the proposed improved strategy decreases from 15 kHz to 9.3 kHz. The frequency reduction is 38%, which effectively reduces the high-frequency switching loss and device stress.

In summary, fixing a single sequence limits the optimization potential of the controller, while the multiple sequence strategy enhances the possibility of "multi-step prediction and rolling optimization" for model predictive control. By designing eight switching sequences in the same sector, the proposed improved FSS-MPC strategy is able to realize a dynamic trade-off between inductor current ripple magnitude and switching loss. The multiple sequences expand the search space of the controller, fully utilize the flexibility of the limited switching sequences, and enable the system to automatically select the optimal sequence, thus improving the overall performance.

6. CONCLUSION

To address the issue of large inductor current ripple in the existing finite switching sequence model predictive control strategy for quasi-Z-source inverter, this paper proposes an improved switching sequence model predictive control strategy for qZSI. The research results demonstrate that the proposed strategy shows significant advantages in suppressing current ripple and improving output waveform quality. The main conclusions are as follows:

(1) The timing distribution of the shoot-through state is optimized by dividing the shoot-through time into four equal segments and allocating them to the critical moments when the switch states are about to change in the traditional control strategy. Experimental results show that this strategy reduces the inductor current ripple amplitude by 44% compared to conventional methods, improving the steady-state performance of the system.

(2) A candidate library containing eight optimized switching sequences is designed, and a switching frequency minimization constraint is introduced into the cost function. This strategy not only ensures control performance but also improves the total harmonic distortion of the grid-side current. Experimental results confirm the enhanced output current waveform quality.

ACKNOWLEDGEMENT

This work was supported by the Scientific Research Fund of Hunan Provincial Education Department under Grant Number 24A0395.

REFERENCES

[1] Peng, F. Z., "Z-source inverter," *IEEE Transactions on Industry Applications*, Vol. 39, No. 2, 504–510, Mar.-Apr. 2003.

[2] Xu, S., "Control method of DC chain voltage of Z source inverter," *Industrial Control Computer*, Vol. 33, No. 8, 124–125, 2020.

[3] Dong, S., Q. Zhang, R. Wang, H. Wang, and S. Cheng, "Development of the Z-Source inverters and its key technologies: A review," *Journal of Electrical Engineering*, Vol. 11, No. 3, 1–12, 2016.

[4] Anderson, J. and F. Z. Peng, "Four quasi-Z-source inverters," in *2008 IEEE Power Electronics Specialists Conference*, 2743–2749, Rhodes, Greece, Jun. 2008.

[5] Zhao, R., C. Yuan, C. Xuan, Q. Li, H. Xu, and Q. Yan, "Forced excitation converter for DFIG-based wind turbine based on variable-structure quasi-Z-source," *Automation of Electric Power Systems*, Vol. 45, No. 19, 181–191, 2021.

[6] Liu, Z., G. Du, and F. Du, "Research status and development trend of finite control set model predictive control in power electronics," *Transactions of China Electrotechnical Society*, Vol. 32, No. 22, 58–69, 2017.

[7] Yao, X. L., C. W. Ma, J. F. Wang, and C. Huang, "Robust model predictive current control for PMSM based on prediction error compensation," in *Proceedings of the CSEE*, Vol. 41, No. 17, 6071–6081, 2021.

[8] Vazquez, S., J. I. Leon, L. G. Franquelo, J. Rodriguez, H. A. Young, A. Marquez, and P. Zanchetta, "Model predictive control: A review of its applications in power electronics," *IEEE Industrial Electronics Magazine*, Vol. 8, No. 1, 16–31, 2014.

[9] Rodriguez, J., M. P. Kazmierkowski, J. R. Espinoza, P. Zanchetta, H. Abu-Rub, H. A. Young, and C. A. Rojas, "State of the art of finite control set model predictive control in power electronics," *IEEE Transactions on Industrial Informatics*, Vol. 9, No. 2, 1003–1016, 2013.

[10] Chen, W., S. Zeng, G. Zhang, T. Shi, and C. Xia, "A modified double vectors model predictive torque control of permanent magnet synchronous motor," *IEEE Transactions on Power Electronics*, Vol. 34, No. 11, 11 419–11 428, 2019.

[11] Zhang, Y. and H. Yang, "Two-vector-based model predictive torque control without weighting factors for induction motor drives," *IEEE Transactions on Power Electronics*, Vol. 31, No. 2, 1381–1390, 2016.

[12] Xu, Y., J. Wang, B. Zhang, and Q. Zhou, "Three-vector-based model predictive current control for permanent magnet synchronous motor," *Transactions of China Electrotechnical Soci-*

ety, Vol. 33, No. 5, 980–988, 2018.

[13] Tarisciotti, L., P. Zanchetta, A. Watson, S. Bifaretti, and J. C. Clare, "Modulated model predictive control for a seven-level cascaded H-bridge back-to-back converter," *IEEE Transactions on Industrial Electronics*, Vol. 61, No. 10, 5375–5383, 2014.

[14] Yeoh, S. S., T. Yang, L. Tarisciotti, C. I. Hill, S. Bozhko, and P. Zanchetta, "Permanent-magnet machine-based starter-generator system with modulated model predictive control," *IEEE Transactions on Transportation Electrification*, Vol. 3, No. 4, 878–890, 2017.

[15] Li, T., X. Sun, Z. Yang, and G. Lei, "Simplified two-step model predictive control with fast voltage vector search," *IEEE Transactions on Industrial Electronics*, Vol. 72, No. 4, 3303–3312, 2025.

[16] Hu, C., X. Sun, Y. Zhang, T. Rui, Z. Yin, and Z. Feng, "Optimal switching sequence model predictive current control for grid connected inverter," *Electric Machines and Control*, Vol. 28, No. 8, 135–142, 2024.

[17] Li, J., B. Liu, W. Xia, and W. Song, "Model predictive flux control for permanent magnet synchronous machine based on switching sequence," *Journal of Power Supply*, Vol. 20, No. 4, 146–154, 2022.

[18] Ma, J., W. Song, and X. Feng, "A model predictive direct power control of single-phase three-level PWM rectifiers," *Proceedings of the CSEE*, Vol. 36, No. 4, 1098–1105, 2016.

[19] Xiao, H., S. Wei, Q. Guo, *et al.*, "Model predictive control strategy for PWM rectifier with optimized switching sequence," *Transactions of China Electrotechnical Society*, Vol. 37, No. 14, 3665–3675, 2022.

[20] Li, T., X. Sun, G. Lei, Y. Guo, Z. Yang, and J. Zhu, "Finite-control-set model predictive control of permanent magnet synchronous motor drive systems — An overview," *IEEE/CAA Journal of Automatica Sinica*, Vol. 9, No. 12, 2087–2105, 2022.

[21] Cheng, J., X. Y. Xiao, J. P. Ma, X. Y. Yang, Y. F. You, and Z. H. Cao, "Finite switching sequence model predictive direct power control of a three-phase energy-stored Quasi-Z-source grid-connected inverter," *Power System Technology*, Vol. 44, No. 5, 1647–1655, 2020.

[22] Kamoshida, N., R. Iijima, T. Isobe, and H. Tadano, "Loss analysis of quasi Z-source inverter with Superjunction-MOSFET," *Electrical Engineering in Japan*, Vol. 205, No. 2, 54–61, 2018.